CrossMark

ORIGINAL PAPER

Light expanded clay aggregate (LECA) as a support for TiO$_2$, Fe/TiO$_2$, and Cu/TiO$_2$ nanocrystalline photocatalysts: a comparative study on the structure, morphology, and activity

Somayeh Sohrabi[1] · Faranak Akhlaghian[1]

Abstract In this work, TiO$_2$ and doped TiO$_2$ photocatalysts (Fe/TiO$_2$ and Cu/TiO$_2$) were synthesized by the sol–gel method. The main objective of this study was to investigate the influence of dopants on the structure, morphology, and activity of the catalysts in powder and immobilized states. XRF, XRD, and SEM methods were used to characterize the catalysts. The structure and phase distribution of the nanocrystalline powders were identified by XRD. Nanoparticles crystallite size and the degree of crystallinity were affected by doping. The anatase contents of catalysts were achieved as follows: TiO$_2$ (5.89 %) < Fe/TiO$_2$ (42.17 %) < Cu/TiO$_2$ (70.28 %). It was indicated that the activity of the catalysts strongly depends on the anatase content. Under the same circumstances, copper-modified TiO$_2$ exhibited a twofold higher photocatalytic activity compared with TiO$_2$. The nanostructured catalysts were immobilized on light expanded clay aggregate (LECA) granules in order to investigate the effect of a novel support on the activity of the catalysts. Morphological changes are recognizable in the SEM images. Activity tests indicated that the best catalytic performance was assigned to Cu/TiO$_2$/LECA. After 120 min of irradiation, 61 % degradation of phenol in synthetic wastewater was achieved. The high photocatalytic activity of Cu/TiO$_2$/LECA confirms that LECA is as an excellent support.

Introduction

Phenol is considered as one of the most important organic contaminants; its major sources in aquatic environment are industrial wastewaters including paint, pesticides, coal conversion, polymeric resin, petroleum, and petrochemical industries. Phenol is reputed for its bioresistance and acute toxicity. Among numerous methods that have been recommended for the degradation of phenolic compounds, photocatalytic treatment is the most effective and economical technology [1–3]. Titanium dioxide (TiO$_2$) has attracted considerable attention mainly because of its high photocatalytic activity, environmental-friendly nature, and the relatively low cost [4]. Several modification methods have been applied to enhance the photocatalytic activity of TiO$_2$. The deposition of nanosized metal particles on TiO$_2$ has proven to be beneficial for improving the efficiency of photocatalytic reactions involved in the degradation of organics. Since these nanoparticles act as a sink of electrons, they inhibit the recombination of electron and hole pairs [5, 6]. Lorret et al. [6] reported that the addition of tungsten drastically improved the photocatalytic activity of TiO$_2$, where the activity was measured via degradation of methylene blue (MB) in aqueous solution. Yean Ling Pang and Ahmad Zuhairi Abdullah prepared Fe-doped titanium dioxide nanotubes using sol–gel followed by hydrothermal method; the activity was evaluated based on the oxidation of rhodamine B under ultrasonic irradiation [7]. Huang et al. [8] concluded that CuO/TiO$_2$ is an active and stable catalyst for CO oxidation. In order to have sufficient separation of the catalyst from aqueous

✉ Somayeh Sohrabi
sohrabisomayeh@yahoo.com; e.sohrabi89@gmail.com

Faranak Akhlaghian
frnakh@yahoo.com

[1] Department of Chemical Engineering, Faculty of Engineering, University of Kurdistan, Sanandaj, Iran

solution and to reuse it, the application of nanosized catalyst, which is suspended in solution, is preferred to be limited. In fact, the application of an appropriate support for catalyst immobilization is of high importance. Various materials have been tested as the substrate for catalysts such as glass, silica, pumice granules, perlite stone, and stainless steel [3, 4]. Haileyesus Tedla et al. applied synthetic zeolite as a support for $ZnO/Fe_2O_3/MnO_2$ composite. They reported high efficiency for the degradation of methylene blue (MB) and real sewage sample [9]. Human society has been using clays and clay minerals since the Stone Age, but recently in line with the rapid advances of nanotechnology, the attention toward clays is focused upon their uses in adsorption, catalysis, and biology [10]. Vaccari [11] stated in 1999 that the application of clays in environmental catalysis would have a promising future. Hassan et al. [12] evaluated the catalytic performance of Ni (II) and Cu (II) phthalocyanines, immobilized on bentonite clay surface. Sharifnia et al. studied the photocatalytic degradation of ammonia using LECA granules as a substrate for their catalyst. The chemical composition of LECA by XRF analysis disclosed that SiO_2 is the major mineral and Al_2O_3 and Fe_2O_3 are present as minor minerals. Meanwhile, some trace minerals were also detected in this natural material [13]. Zarrabi et al. have used LECA for defluoridation of water and reported some of the properties of lightweight expanded clay aggregate (LECA) such as low density, high porosity, and thermal resistance (up to 1000 °C). The porous structure of LECA along with its low density facilitates its floatability [14].

In this research study, TiO_2, Fe/TiO_2, and Cu/TiO_2 photocatalysts were synthesized by sol–gel method. The structure and morphology of the catalysts were scrutinized by XRF, XRD, and SEM techniques. Moreover, the activity of the catalysts was compared in suspended and immobilized modes. Light expanded clay aggregate (LECA) was applied as a support to immobilize TiO_2, Fe/TiO_2, and Cu/TiO_2 photocatalysts.

Materials and methods

Materials

To prepare Cu/TiO_2 and Fe/TiO_2 photocatalysts, titanium isopropoxide (98 %), Cu $(NO_3)_2 \cdot 3H_2O$ (99 %), Fe $(NO_3)_3 \cdot 9H_2O$ (98 %) were used as the precursors for the titanium, copper, and iron, respectively. LECA is a special type of clay, which has been pelleted and fired in a rotary kiln at a very high temperature (with grain size of 4–10 mm). LECA is considered a silicate compound. It was provided by Azarbayjani Company, Kermanshah, Iran. It

was crashed and washed with tap water in order to remove the dust. Subsequently, it was heated at 100 °C, until the weight became constant. Moreover, ethanol (96 %) and nitric acid (65 %) were used for the synthesis of the catalysts and H_2O_2 (30 wt%) and phenol (99 %) were used in the phenol photodegradation experiments. The chemicals were purchased from Merck Company and used without further purifications. Distilled water was used through the experiments.

Methods

### Synthesis of Cu/TiO_2 and Fe/TiO_2 photocatalysts

Step 1: Based on sol–gel method, titanium isopropoxide (TIP) was added to double-distilled water with the molar ratio of 1:100 (TIP to water). The mixture has been stirring and heating up to 85 °C. Step 2: At that temperature, a specified amount of nitric acid was added so that the molar ratio of TIP to nitric acid was 1:0.07. Meanwhile, a solution of 2 wt% of Cu, which was prepared by dissolving Cu $(NO_3)_2 \cdot 3H_2O$ in ethanol, was added. In case of Fe/TiO_2 photocatalyst, a solution of 2 wt% of Fe, which was obtained by dissolving Fe $(NO_3)_3$ $9H_2O$ in ethanol, was used. Step 3: The mixture was kept under reflux at 85 °C for 24 h. Step 4: The obtained gel was dried at 100 °C. Step 5: The dried gel calcination was conducted at 600 °C for 2 h. The experimental data on the choice of calcination temperature are given in [15]. Finally, the powder was crushed and sieved into 60–90 μm.

Immobilization

LECA was applied as the support for TiO_2, Fe/TiO_2, and Cu/TiO_2 photocatalysts. The procedure of Cu/TiO_2/LECA preparation is presented in Fig. 1. The first three steps of Cu/TiO_2/LECA preparation method, which consist of the preparation of a homogenous mixture from the precursors, the hydrolysis of Ti alkoxide, and the formation of sol, were the same as the synthesis method of Cu/TiO_2 photocatalyst. Afterward, LECA granules were added to the obtained sol. Step 4: the LECA granules, which had adsorbed sufficient sol, were filtered and dried at 100 °C. Step 5: Finally, the calcination process was carried out at 600 °C for 2 h. Hereby, TiO_2, Fe/TiO_2, and Cu/TiO_2 were immobilized and coated on LECA.

Characterization

Copper and iron content of the catalysts were measured by X-ray fluorescence (XRF) spectrometer (Spectro X-Lab Pro). TiO_2 and modified TiO_2 powders were
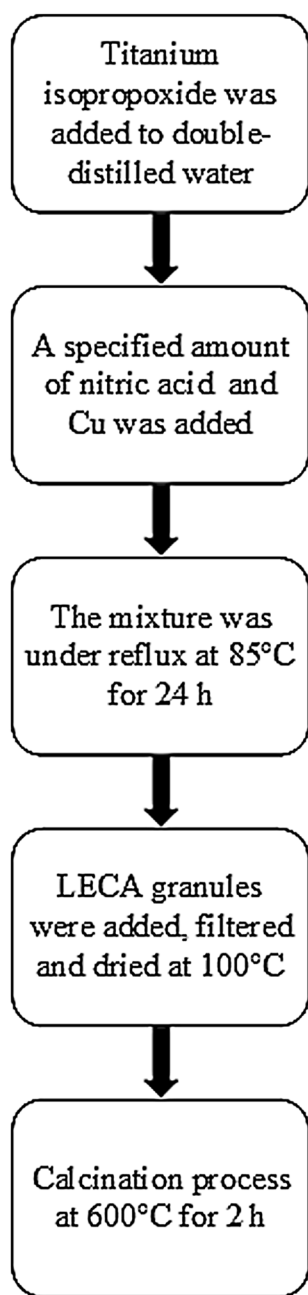
Fig. 1 The synthesis procedure of Cu/TiO$_2$/LECA photocatalyst

characterized by X-ray diffraction (XRD) using X'Pert MPD diffractometer with Cu Kα radiation at 40 kV and 40 mA. The XRD patterns were collected from 5° to 80° in 2θ at a scan rate of 0.2°/s. The morphology of the catalysts was investigated by field emission scanning electron microscopy of FESEM of the TSCAN Company on the acceleration voltage of 15.0 kV. The porosity of the catalysts was investigated using Micrometrics ASAP 2010. Before measuring nitrogen adsorption, the catalyst was degassed at 300 °C for 6 h.

Photocatalytic experiments

The catalyst was added to a phenol solution (200 ppm), which was selected as the synthetic wastewater. Hydrogen peroxide (H_2O_2: 12.5 ml, 30 wt%) was added to the solution as an oxidizing agent. The amounts of catalyst loading, initial phenol concentration, and H_2O_2 dosage were investigated and optimized in one of our previous works [16]. From our optimization experiments for Cu/TiO$_2$ [17], it can be concluded that the optimum Cu/TiO$_2$ dosage is 0.5 g/l. In addition, according to another work of us [16], the optimum dosage for Fe/TiO$_2$ dosage is 0.5 g/l. Accordingly, based on the results obtained by the two papers, the dosages of Cu/TiO$_2$ and Fe/TiO$_2$ in suspended photocatalytic experiments were determined to be 0.5 g/l.

To be able to have a rational judgment on the competitive performance of the catalysts in suspended and immobilized states, we decide to adjust the dosages of Cu/TiO$_2$/LECA and Fe/TiO$_2$/LECA catalysts so as to obtain 0.5 g/l dosage for Cu/TiO$_2$ in Cu/TiO$_2$/LECA (likewise for Fe/TiO$_2$ in Fe/TiO$_2$/LECA). It means that LECA granules were weighed before absorbing sol and after the calcination process. The difference between these two values reveals the Cu/TiO$_2$ amount, which is immobilized on LECA (likewise for Fe/TiO$_2$ in Fe/TiO$_2$/LECA). Since in each experiment 200 ml of phenol solution is used, 0.1 g of catalyst is applied to attain 0.5 g/l dosage. To immobilize 0.1 g of Fe/TiO$_2$ on LECA 3.96 g of the substrate was needed, while for Cu/TiO$_2$ the required amount of LECA is lower (3.58). This shows superior immobilization of Cu/TiO$_2$ on LECA.

A magnetic stirrer was used to provide uniform conditions in the reacting solution. The illumination is conducted by a UV lamp (with light intensity of 757.38 mW/cm^2), which was fixed 19.5 cm over the batch photoreactor of cylindrical shape (Pyrex vessel capacity: 2L). The setup was in a chamber, and it was shielded by aluminum foil during the reaction time to prevent the interference from outside light.
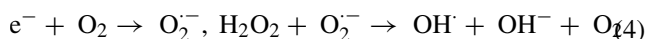
Analytical methods

All the experiments were carried out at ambient temperature. After 2 h of reaction, the mixture was centrifuged and the absorbance of the supernatant was measured at 270 nm using a Specord 210 UV spectrometer. The experiments should be repeated for the blank. All the conditions in the blank were the same as the sample, but the blank had no catalyst. The activity of photocatalysts was evaluated by determining the phenol degradation percentage. The concentration of phenol in the solution was measured using the Beer–Lambert law, and the degradation of phenol was calculated using the following equation [16]:

Degradation $\% = 100 \times [(A_0 - A)/A_0]$ (1)

where A_0 and A are absorbance of blank and sample, respectively.

Mechanism

In the photocatalytic degradation process, an organic pollutant is destroyed in the presence of an oxidizing agent and a semiconductor, which is irradiated by an energetic light source. As the result of sufficient illumination with UV lamp, an electron from the valence band migrates to the conduction band leaving behind an electron vacancy (hole) in the valence band. The generated hole in the valence band can produce hydroxyl radicals, and subsequently, OH radicals oxidize the organic material. The photogenerated e^- and h^+ are vigorous oxidizing and reducing agents, and their reactions are, respectively, as follows:

$$H_2O + h^+ \rightarrow OH^. + H^+ \qquad (2)$$

$$e^- + H_2O_2 \rightarrow OH^. + OH^- \qquad (3)$$

$$e^- + O_2 \rightarrow O_2^{.-}, \ H_2O_2 + O_2^{.-} \rightarrow OH^. + OH^- + O_2 \quad (4)$$

Equation (2) expresses the hydroxyl radicals generation by the oxidation step, in which positive holes react with absorbed water. The reduction step leads to the hydroxyl radical generation through direct and indirect routes; the direct way, which is stated in Eq. (3), is the reaction of electrons with H_2O_2. The indirect way, which is summarized in Eq. (4), composes of two steps: First, e^- is transferred to the adsorbed oxygen of the modified catalyst (Cu/TiO$_2$, Fe/TiO$_2$), which produces superoxide anions and then O_2^- reacts with H_2O_2 resulting in $^.$OH generation. When reduction and oxidation do not advance simultaneously, there would be an electron accumulation in the conduction band. Thereby, this can increase the rate of recombination of e^- and h^+. Since the recombination causes energy waste, it should be prevented to ensure efficient photocatalysis. The role of dopant in photocatalysis is in keeping the charges separate through trapping the electrons of TiO$_2$ conduction band and consequently avoiding the recombination of electrons and holes [2, 18]. Cu^{2+} and Fe^{3+}, which are absorbed on the TiO$_2$ surface, can act as electron trapping centers. Thus, they increase the electron–hole pair separation efficiency.

Results and discussion

XRF

Chemical composition of the doped catalysts, which was evaluated by XRF analysis, is indicated in Table 1. Given

Table 1 XRF analysis of Fe/TiO$_2$ and Cu/TiO$_2$ photocatalysts

Sample	TiO$_2$ (wt%)	CuO (wt%)	Fe$_2$O$_3$ (wt%)	Loss on ignition (wt%)
Fe/TiO$_2$	95.71	–	0.2	4.08
Cu/TiO$_2$	99.47	0.24	–	0.3

that the method of synthesis, all the materials used and their quantities, is the same for the two catalysts (Cu/TiO$_2$ and Fe/TiO$_2$), only the type of dopant is different (a solution of 2 wt% of Cu was used in step 2 of Cu/TiO$_2$ synthesis, and likewise a solution of 2 wt% of Fe for Fe/TiO$_2$ synthesis). Under the current circumstance, chemical composition of the doped catalysts indicates that the ratio of CuO/TiO$_2$ is 0.24 % and the ratio of F$_2$O$_3$/TiO$_2$ is 0.2 %. Higher CuO loading in Cu/TiO$_2$ suggests better embedment of the dopant in the TiO$_2$ lattice, and accordingly, it possesses more active sites.

XRD

The X-ray powder diffraction was used to determine the crystalline phases present in the samples. XRD patterns of pure TiO$_2$, Fe/TiO$_2$, and Cu/TiO$_2$ are shown in Fig. 2. In the XRD pattern of pure titanium dioxide, the peak at 29.5090° is attributed to the anatase phase (JCPDS 21-1272), and the peaks at 32.0095°, 42.1696°, and 64.0611° are attributed to rutile (JCPDS 21-1276). These results imply that both rutile and anatase phases exist in pure TiO$_2$. In the XRD pattern of Cu/TiO$_2$, in addition to the peaks, corresponding to rutile and anatase phases (JCPDS 21-1272 and 21-1276), there is a peak at 63.52°, which corresponds to CuO (JCPDS 48-1548). Additionally, in the pattern of Fe/TiO$_2$, along with the peaks belonging to rutile and anatase phases, two peaks at 56.51° and 65.02° are recognized, which correspond to Fe$_2$O$_3$ (JCPDS file no. 39-1346). Phase distribution of samples is estimated by Spurr–Myers correlation where the weight percent of anatase is given by:

$$X_A = (1/(1 + 1.26(I_R/I_A))) \qquad (5)$$

where "X" denotes the weight fraction, "I" denotes the intensity of the strongest reflection, and the subscripts "A and R" denote the anatase and rutile phases, respectively. The anatase content is estimated by Eq. (5). The rutile content can then be determined by a subtraction [19].

The portions of anatase and rutile phases, which are calculated according to Eq. (5), are presented in Table 2. As can be seen, more than 90 % of titanium dioxide crystals are in the rutile phase, while Fe/TiO$_2$ is composed of 42.17 % of anatase and Cu/TiO$_2$ is mainly made up of anatase structure (70.28 %). Thus, the crystallization of a catalyst, especially the ratio of anatase to rutile, is

Fig. 2 XRD patterns of pure and modified titanium dioxide (anatase to rutile ratio: TiO_2 (0.0626) < Fe/TiO_2 (0.7292) < Cu/TiO_2 (2.3647))
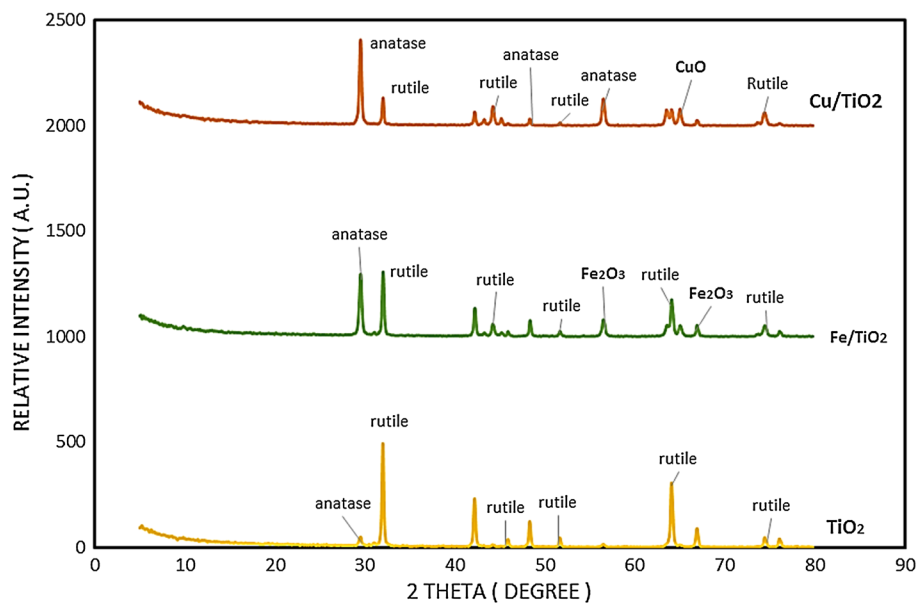
Table 2 The results obtained by XRD for TiO_2 and Cu/TiO_2 photocatalysts

Samples	Anatase (wt%)	Rutile (wt%)	A/R	D_{ave} (nm)	C (%)
TiO_2	5.89	94.11	0.0626	113.99	81.21
Fe/TiO_2	42.17	57.83	0.7292	80.00	73.32
Cu/TiO_2	70.28	29.72	2.3647	71.25	73.00

affected by dopants. Moreover, it is observed that the existence of dopants decreases anatase to rutile transformations. The XRD patterns enunciate that the catalysts are composed of both anatase and rutile phases. Juang et al. indicated that high catalytic activity is associated with the crystalline structures containing both anatase and rutile. In other words, the co-existence of the two phases leads to a synergistic effect [20]. A higher content of rutile phase is related to a lower photocatalytic activity [2, 21, 22]. Another important point, which lies in the XRD patterns, is that as the result of copper oxide incorporation into the crystalline structure of TiO_2, the intensity of anatase peak is increased and the intensity of rutile peaks is abated. It can be observed that the dopants retard anatase to rutile transformations. A higher anatase content indicates higher catalytic activity. Accordingly, Cu/TiO_2 that is primarily composed of highly active anatase structure has the potential to be an outstanding photocatalyst. The experimental results confirm the existence of a relationship between anatase content and catalytic activity.

The Scherrer formula is used to estimate the crystallite size of the nanoparticles, where "D" is the crystallite size, "K" is a correction factor, which is related to shape, taken as 0.89, "λ" is wavelength of X-ray radiation used (0.15406 nm), "β" is the line width at half-maximum peak height, after subtraction from equipment broadening, and "θ" is the diffraction angle [23].

$$D = (K\lambda)/(\beta \cos\theta) \tag{6}$$

Since the samples are made up of both anatase and rutile phases, crystallite sizes of samples should be the average according to the following equation:

$$D_{ave} = D_A(I_A/(I_A + I_R)) + D_R(I_R/(I_A + I_R)) \tag{7}$$

Crystallinity degree is defined as the crystalline portion of a sample divided by the sum of both crystalline and amorphous portions.

$$C = (I_C/(I_C + I_A)) \times 100 \tag{8}$$

where "C" is the crystallinity degree and "I_C and I_A" are diffracted X-ray radiations of crystalline and amorphous portions of the samples, respectively [24].

Nanoparticles crystallite size based on Eq. (7) and the degree of crystallinity based on Eq. (8) are calculated and given in Table 2. From the results of Table 2, it is inferred that the crystallinity and likewise the crystallite size are reduced as the dopant is embedded into the TiO_2 lattice. It is originated from the fact that the order of TiO_2 lattice is disturbed by the dopant, in fact because of the different ionic radius of Ti^{4+} and Fe^{3+} or Cu^{2+}. The source for numerical values of ionic radii is the paper by Shannon [25]. According to the so-called database, most reliable numerical value for ionic radii of Fe^{3+}, Cu^{2+}, and Ti^{4+} is 0.645, 0.57, and 0.605, respectively. Thereupon, the disorder imposed to the lattice because of dopants incorporation
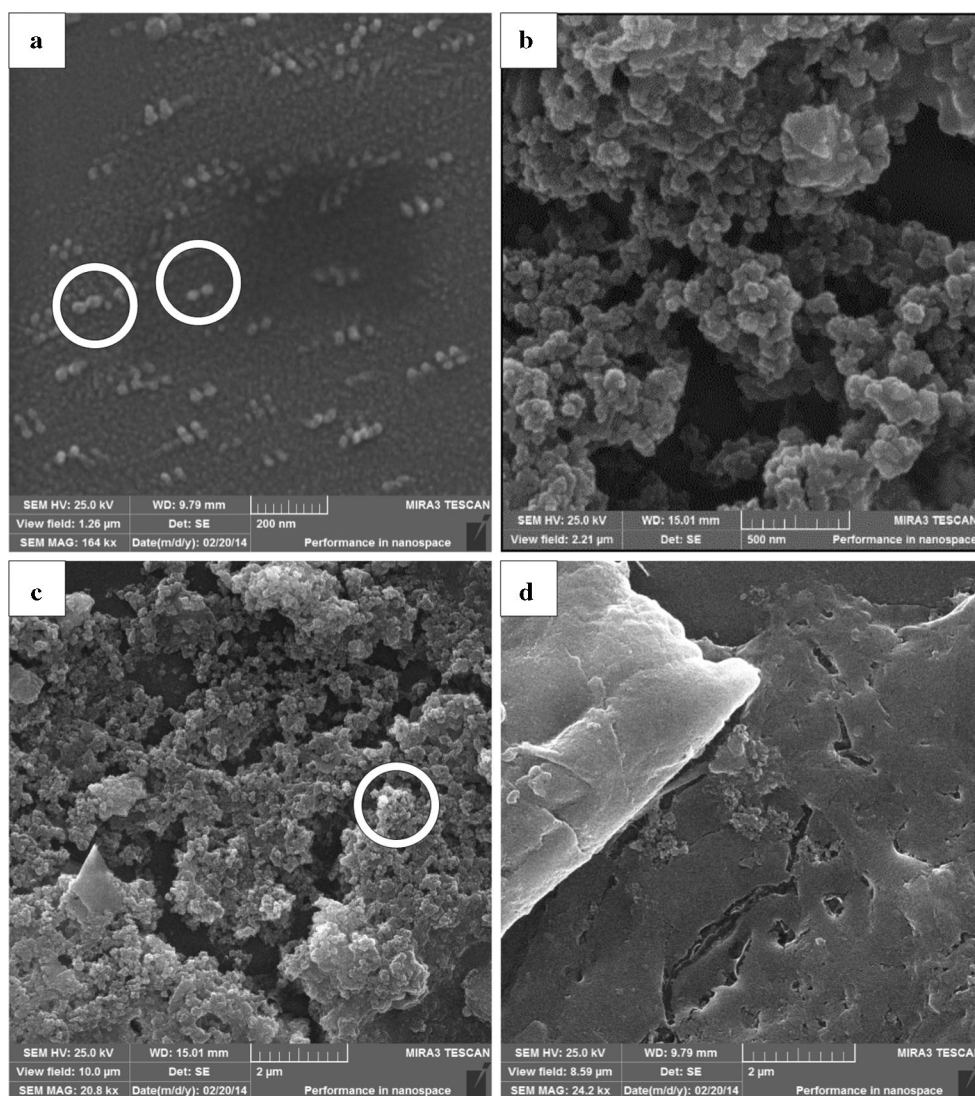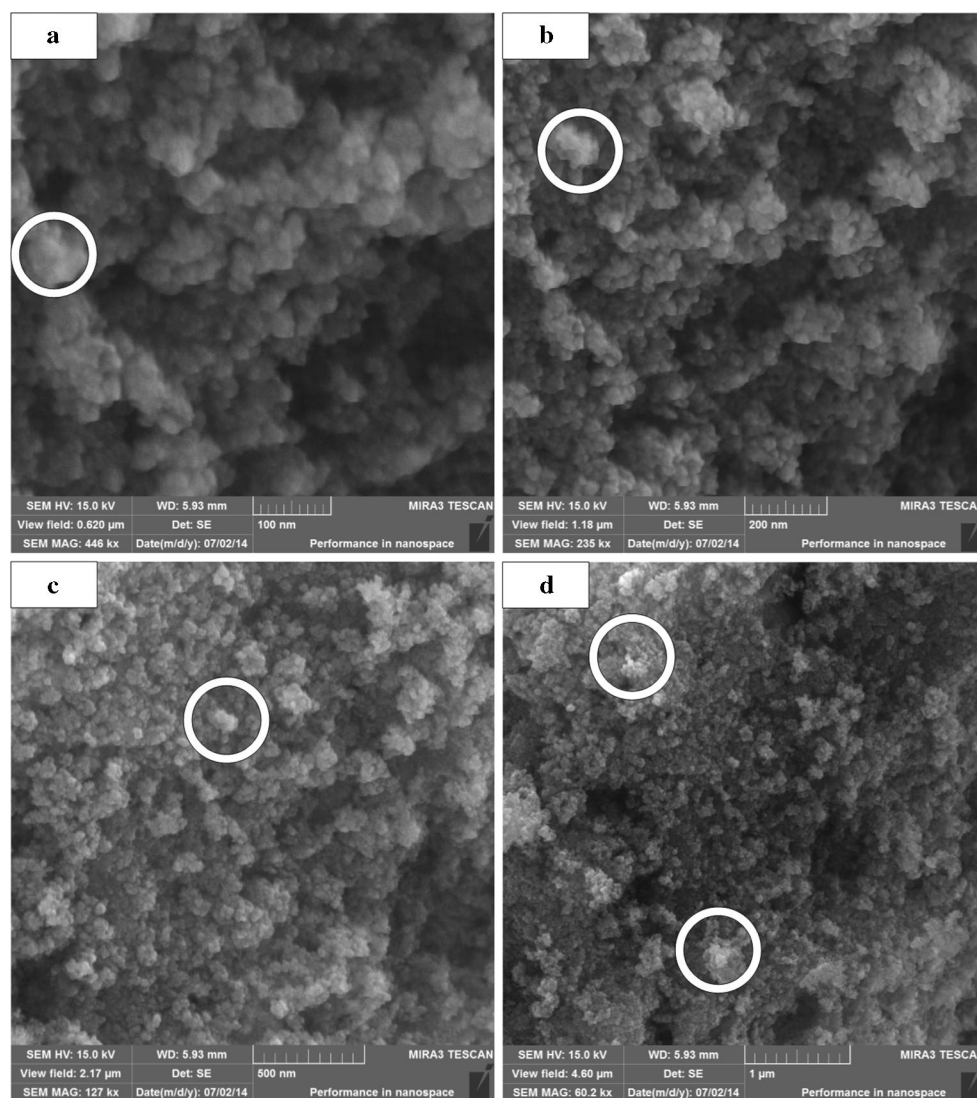
Fig. 3 The SEM images of the Fe/TiO$_2$

leads to the formation of defects. Defects are considered as amorphous. The more defects form, the less crystalline phases exist, and crystallinity degrees of the samples are decreased. In addition, XRD results, which are presented in Table 2, indicate that the existence of dopants retards the crystallization of samples decreasing anatase to rutile transformations. Thus, the crystallinity degree is reduced as the dopant is embedded into the TiO$_2$ lattice.

SEM

Figures 3, 4b, and 5 illustrate the scanning electron micrographs (SEM) of Fe/TiO$_2$, Cu/TiO$_2$, and Cu/TiO$_2$/LECA photocatalysts, respectively. It is quite evident that the surface morphology of iron-modified TiO$_2$ is different from that of copper-modified TiO$_2$. Since the synthesis methods

are identical, it can be concluded that dopants are responsible for the morphological changes. The scales of the images of Fe/TiO$_2$ in Fig. 3 range from 200 nm to 2 µm. Figure 3a displays that the Fe$_2$O$_3$ nanoparticles are distributed evenly on the TiO$_2$ smooth surface. Bright spots, which are representative of iron oxide particles, are marked by white rings. Figure 3b, c, and d images exemplify the porosity of the catalyst. The images of Fig. 4, ranging from 100 nm to 1 µm, correspond to Cu/TiO$_2$. The brilliant spots are representative of copper oxides, which are homogenously incorporated into the TiO$_2$ lattice. It is of high importance that the morphology of CuO nanoparticles in Cu/TiO$_2$ photocatalyst is different from Cu/TiO$_2$/LECA photocatalyst. Therefore, SEM images of Cu/TiO$_2$/LECA were studied over a wider range (500 nm–50 µm). It is indicated from the images of Fig. 5a–d that Cu/TiO$_2$

Fig. 4 The SEM images of the Cu/TiO$_2$

covers the LECA surface with a uniform flaky layer. Active sites of the catalyst are depicted as brilliant spots, which are representative of CuO particles marked by white rings. Moreover, the microporous structure of LECA granules is depicted in the images of Fig. 5e–h. The high porosity of LECA suggests that it can be applied as an appropriate support. The copper-modified titanium dioxide photocatalyst, which was coated on LECA, simultaneously benefits from the high activity of Cu/TiO$_2$ and the high porosity of LECA.

The SEM images are different regarding dopant covering and loading in TiO$_2$ structure. CuO is found more abundantly in SEM images compared to Fe$_2$O$_3$; the existence of bright spots is more frequent in Cu/TiO$_2$, but in one aspect they all are alike each other and this is the fact that the nanocatalysts (Cu/TiO$_2$ and Fe/TiO$_2$) are porous materials.

Specifically, the microporosity of LECA and mesoporosity of Cu/TiO$_2$ and Fe/TiO$_2$ are evident in the SEM images. In the SEM images of Cu/TiO$_2$/LECA, pores in the micrometers scale are obviously detectable, and the SEM images of Cu/TiO$_2$ and Fe/TiO$_2$ pores in nanodimensions are well depicted.

N$_2$ adsorption/desorption isotherm

Nitrogen adsorption/desorption isotherm for Fe/TiO$_2$ catalyst is shown in Fig. 6. The isotherm shape confirms that Fe/TiO$_2$ catalyst is mesoporous. According to IUPAC classification, Fe/TiO$_2$ corresponds to type IV, which represents mesoporous solids, and regarding hysteresis, it belongs to type H2. Catalysts with H2-type hysteresis have inkbottle pores [26]. As it is noted in "Synthesis of Cu/TiO$_2$ and Fe/
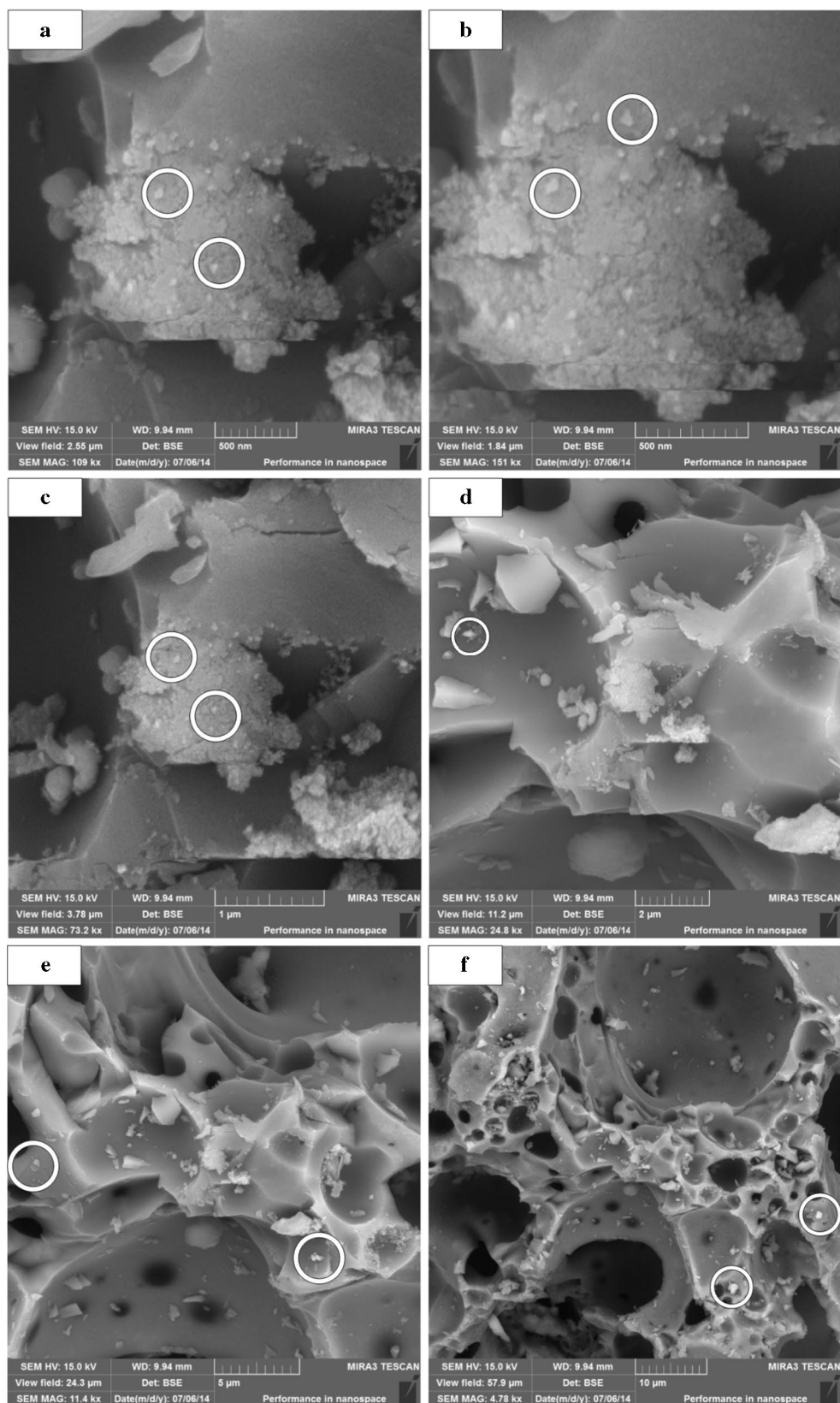
Fig. 5 The SEM images of the Cu/TiO$_2$/LECA
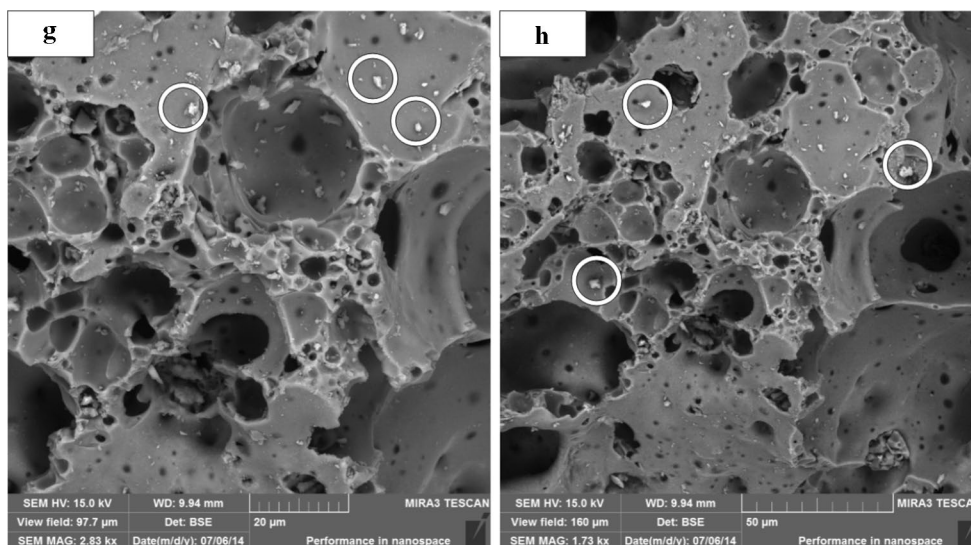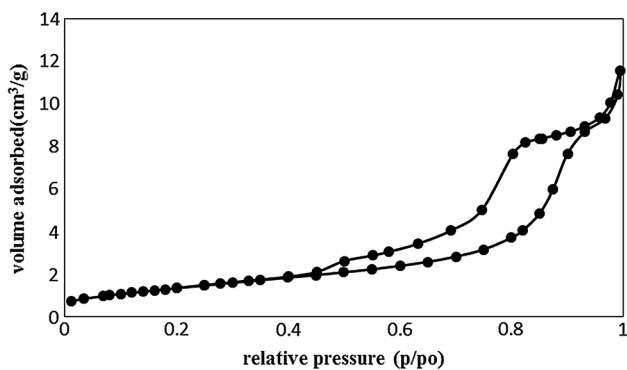
Fig. 5 continued

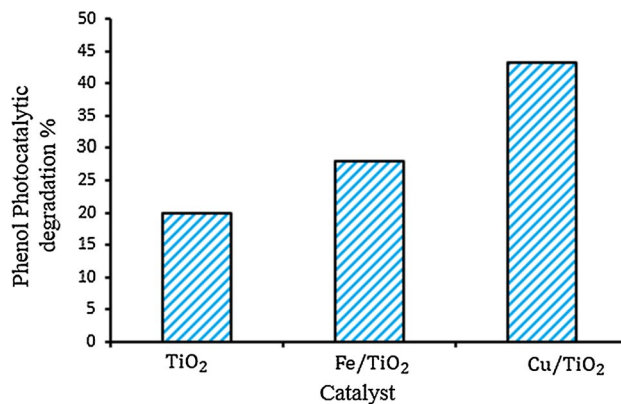**Fig. 6** Nitrogen adsorption/desorption isotherm for Fe/TiO$_2$ catalyst

Fig. 7 The effect of doping on the photocatalytic activity of TiO$_2$ (the catalysts are suspended in solution)

TiO$_2$ photocatalysts" section, the titanium precursor and the synthesis method for Cu/TiO$_2$ and Fe/TiO$_2$ photocatalysts are the same and the whole quantities and ratios of materials kept constant. In summary, all the conditions, which affect porosity, are the same. It can be concluded that Fe/TiO$_2$ and Cu/TiO$_2$ nanocatalysts are porous materials. The results are in agreement with [27].

LECA (the applied substrate in this work) is a commercial product, which is manufactured worldwide, and accordingly, its properties such as low density, high porosity, and high surface area are well known. Furthermore, there are numerous articles [28–34], which support its porosity and high surface area.

Activity tests of suspended catalysts

Recently, many researchers have focused on enhancing the photocatalytic activity of TiO$_2$. As an illustration,

doping TiO$_2$ with nonmetals like nitrogen and carbon was reported. Moreover, metallic nanoparticles have been used to improve the catalytic activity of TiO$_2$ [6, 35]. A couple of studies reported high photocatalytic activity of Cu-doped TiO$_2$ [36–39]. Tryba [40] observed that photoactivity of Fe–C–TiO$_2$ was higher than TiO$_2$. In this work, phenol photocatalytic degradation was experimentally investigated to evaluate the activity of TiO$_2$, Fe/TiO$_2$, and Cu/TiO$_2$ photocatalysts. The catalysts were applied in the powder form, and the powders have been suspended in the phenol solution with the aid of magnetic stirrer. The catalyst loading was the same for each experiment (0.5 g/l). The results are given in Fig. 7. Phenol degradation efficiency was 19.98 % for TiO$_2$, 27.87 % for Fe/TiO$_2$, 43.21 % for Cu/TiO$_2$. The results assert that introduction of iron and copper in the titanium dioxide lattice results in enhancing its photocatalytic

activity. It is notable that copper has a more pronounced effect compared to iron. Cu-loaded TiO_2 exhibits a two-fold higher photocatalytic activity compared with TiO_2 under the same conditions, which can be attributed to the chemical synergy, which is originated from the interaction between CuO and TiO_2. This brings about suitable incorporation of copper oxide particles in the TiO_2 lattice.

The XRD, XRF, SEM are consistent with the experimental results asserting higher photocatalytic activity of Cu/TiO_2. First, XRD results validate the higher catalytic activity of Cu/TiO_2. Higher anatase content of Cu/TiO_2 enunciates that it has higher catalytic activity in comparison with Fe/TiO_2. In addition, it is evident in the XRD pattern that anatase peak has intensified more noticeably once TiO_2 is doped with Cu. Second, XRF analysis also confirms higher catalytic activity of Cu/TiO_2. Chemical composition of the doped catalysts indicates that the ratio of CuO/TiO_2 is 0.24 % and the ratio of F_2O_3/TiO_2 is 0.2 %. The higher CuO loading in Cu/TiO_2 suggests better incorporation of the dopant in the TiO_2 lattice, and accordingly, Cu/TiO_2 has more active sites, and thus, it validates the higher catalytic activity of Cu/TiO_2. As the final clue in this section, in the SEM images CuO is found more abundantly compared to Fe_2O_3; the existence of bright spots representing active sites are more frequent in Cu/TiO_2.

This finding is consistent with the work of Suen and Adesina [41], who reported excellent activity of $CuO-TiO_2$ catalyst in the degradation of 4-hydroxy nitrobenzene. They attributed the enhanced performance of the catalyst to the co-operative interaction of CuO surface and TiO_2 lattice. They enunciated that this synergetic effect leads to create more active sites. Sato and Taya [37] studied the sterilization of microbial cells, and they concluded that copper component in solid phase (Cu/TiO_2 film) is responsible for the promotion of •OH generation. On the other hand, Shan et al. [42] notified that among the three crystalline forms of TiO_2, anatase tends to be the most stable form at low temperatures (<700 °C). The XRD results confirm that Cu/TiO_2 owing to its higher anatase content can be a more effective catalyst than TiO_2 and Fe/TiO_2.

Activity tests of immobilized catalysts

The application of catalysts in powder form has some drawbacks such as the loss of catalyst and the need for separation technologies to regenerate the catalyst, which are both time- and money-consuming. Moreover, the catalyst loading should be limited; the turbidity of the solution, which is a result of catalyst overuse, leads to scatter the UV light, and thus less sites of catalyst can be activated. Less available surface area, poor reusability,
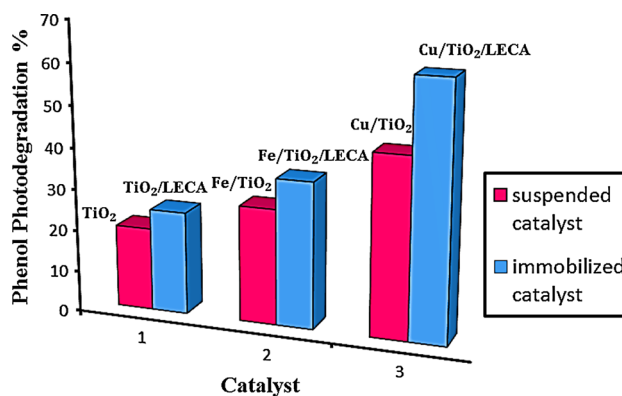
Fig. 8 The effect of LECA as novel substrate on the activity of TiO_2, Fe/TiO_2, and Cu/TiO_2 photocatalysts (the catalysts are immobilized)

and low adsorption ability are some other disadvantages of suspended photocatalysis. To overcome these problems, the immobilization of the catalyst on an appropriate support is recommended [43–45]. The activity of the catalysts in suspended and immobilized states was experimentally compared. The results are presented in Fig. 8. It is observed that the photocatalysts, which are immobilized on LECA, have better performance in phenol degradation in comparison with powder photocatalysts. As an instance, phenol degradation efficiency for Cu/TiO_2 in its powder form is 43.21 %, while the efficiency of 61 % is attained for the LECA-supported Cu/TiO_2. The higher efficiency can be attributed to the enhanced accessible reaction surface provided by the porous structure of LECA. Shan et al. considered the high surface area of a support as a key property for enhancing the activity of a catalyst [41]. Furthermore, floatability of LECA, which is originated from its high porosity, enables the $TiO_2/LECA$, $Fe/TiO_2/LECA$, and $Cu/TiO_2/LECA$ photocatalysts to be exposed to the UV light for a longer time. This causes the activation of more catalytic sites. On the other hand, porous structure can trap light facilitating the photocatalyst activation. It is noted in "Photocatalytic experiments" section that to coat the same amount of catalysts on LECA, for Cu/TiO_2 less LECA was used. The fact that with lower substrate amount, better performance in phenol degradation is observed supports the higher photocatalytic activity of $Cu/TiO_2/LECA$.

Conclusion

Nanocrystalline powders were successfully synthesized by sol–gel method. The XRD results enunciate that the catalysts are composed of both anatase and rutile phases and anatase is the significant phase of Cu/TiO_2. It has been shown that the presence of cation dopants such as

Fe^{3+} and Cu^{2+} in TiO$_2$ lattice is followed by these structural consequences:

1. Decelerating anatase to rutile transformations (anatase peaks have intensified, while rutile peaks have abated in the XRD patterns of the doped catalysts.)
2. Decreasing the crystallite size of the nanoparticles
3. Reducing the nanoparticles crystallinity degree
4. The existence of copper oxide (CuO) in Cu/TiO$_2$ and Fe$_2$O$_3$ in Fe/TiO$_2$ is confirmed by their corresponding peaks in the XRD patterns. The XRF results reveal that the ratio of CuO/TiO$_2$ is 0.24 % and F$_2$O$_3$/TiO$_2$ is 0.2 %. The SEM images of Fe/TiO$_2$ and Cu/TiO$_2$ catalysts declare that the morphological changes arise from difference of the dopants. Moreover, the microporosity of Cu/TiO$_2$/LECA photocatalyst and mesoporosity of Cu/TiO$_2$ and Fe/TiO$_2$ are evident in the corresponding SEM images. The experimental results assert that doping TiO$_2$ with copper will have an outstanding impact on enhancing its photocatalytic activity. The high activity of Cu/TiO$_2$ is considered to arise from high content of anatase and better incorporation of the dopant in the TiO$_2$ lattice. To overcome the problems regarding suspended photocatalytic reactions, the photocatalysts were immobilized on LECA. The high porosity and low density of LECA empower it to be an ideal substrate for photocatalytic processes. It was observed that the photocatalysts which were coated on LECA showed superior catalytic activity compared to the suspended photocatalysts.

References

1. E. Grabowska, J. Reszczynska, A. Zaleska, Mechanism of phenol photodegradation in the presence of pure and modified-TiO$_2$: a review. Water Res. **46**, 5453–5471 (2012). doi:10.1016/j.watres.2012.07.048
2. S. Ahmed, M.G. Rasul, W.N. Martens, R. Brown, M.A. Hashib, Heterogeneous photocatalytic degradation of phenols in wastewater: a review on current status and developments. Desalination **261**, 3–18 (2010). doi:10.1016/j.desal.2010.04.062
3. T. Luenloi, B. Chalermsinsuwan, T. Sreethawong, Photodegradation of phenol catalyzed by TiO$_2$ coated on acrylic sheets: kinetics and factorial design analysis. Desalination **274**, 192–199 (2011). doi:10.1016/j.desal.2011.02.011
4. S. Souzanchi, F. Vahabzadeh, S. Fazel, S.N. Hosseini, Performance of an annular sieve-plate column photoreactor using immobilized TiO$_2$ on stainless steel support for phenol degradation. Chem. Eng. J. **223**, 268–276 (2013). doi:10.1016/j.cej.2013.02.123
5. S. Oros-Ruiz, R. Zanella, B. Prado, Photocatalytic degradation of trimethoprim by metallic nanoparticles supported on TiO$_2$-P25. J. Hazard. Mater. **263**, 28–35 (2013). doi:10.1016/j.jhazmat.2013.04.010
6. O. Lorret, D. Francova´, G. Waldner, N. Stelzer, W-doped titania nanoparticles for UV and visible-light photocatalytic reactions. Appl. Catal. B **91**, 39–46 (2009). doi:10.1016/j.apcatb.2009.05.005
7. Y.L. Pang, A.Z. Abdullah, Effect of low Fe^{3+} doping on characteristics, sonocatalytic activity and reusability of TiO$_2$ nanotubes catalysts for removal of Rhodamine B from water. J. Hazard. Mater. **235–236**, 326–335 (2012). doi:10.1016/j.jhazmat.2012.08.008
8. J. Huang, S. Wang, Y. Zhao, X. Wang, S. Wang, W. Shihua, S. Zhang, W. Huang, Synthesis and characterization of CuO/TiO$_2$ catalysts for low-temperature CO oxidation. Catal. Commun. **7**, 1029–1034 (2006). doi:10.1016/j.catcom.2006.05.001
9. H. Tedla, I.D.T. Kebede, A.M. Taddesse, Synthesis, characterization and photocatalytic activity of zeolite supported ZnO/Fe$_2$O$_3$/MnO$_2$ nanocomposites. J. Environ. Chem. Eng. **3**, 1586–1591 (2015). doi:10.1016/j.jece.2015.05.012
10. C.H. Zhou, J. Keeling, Fundamental and applied research on clay minerals: from climate and environment to nanotechnology. Appl. Clay Sci. **74**, 3–9 (2013). doi:10.1016/j.clay.2013.02.013
11. A. Vaccari, Clays and catalysis: a promising future. Appl. Clay Sci. **14**, 161–198 (1999). doi:10.1016/S0169-1317(98)00058-1
12. S.A. Hassan, F.Z. Yehia, A.A. Hamed, A.A. Zahran, S.M. Solyman, Interaction characteristics controlling catalytic performances of Ni (II) and Cu (II) phthalocyanines immobilized on bentonite clay surface in redox-initiated polymerization of methyl methacrylate in aqueous medium. J. Porous Mater. **18**, 1–11 (2011). doi:10.1007/s10934-009-9350-z
13. Y. Shavisi, S. Sharifnia, M. Zendehzaban, M.L. Mirghavami, S. Kakehazar, Application of solar light for degradation of ammonia in petrochemical wastewater by a floating TiO$_2$/LECA photocatalyst. J. Ind. Eng. Chem. **20**, 2806–2813 (2014). doi:10.1016/j.jiec.2013.11.011
14. M.N. Sepehr, H. Kazemian, E. Ghahramani, A. Amrane, V. Sivasankar e, M. Zarrabi, Defluoridation of water via light weight expanded clay aggregate (LECA): adsorbent characterization, competing ions, chemical regeneration, equilibrium and kinetic modeling. J. Taiwan Inst. Chem. Eng. **45**, 1821–1834 (2014). doi:10.1016/j.jtice.2014.02.009
15. S. Sohrabi, F. Akhlaghian, The effect of fe-loading and calcination temperature on the activity of Fe/TiO$_2$ in phenol degradation, Iran. J. Chem. Chem. Eng. **35**(2), 43–50 (2016)
16. F. Akhlaghian, S. Sohrabi, Fe/TiO$_2$ catalyst for photodegradation of phenol in water. Int. J. Eng. IJE Trans. A Basics **28**, 499–506 (2015). doi:10.5829/idosi.ije.2015.28.04a.02
17. S. Sohrabi, F. Akhlaghian, Modeling and optimization of phenol degradation over copper-doped titanium dioxide photocatalyst using response surface methodology. Process Saf. Environ. Prot. **99**, 120–128 (2016). doi:10.1016/j.psep.2015.10.016
18. L. Sun, J. Li, C.L. Wang, S.F. Li, H.B. Chen, C.J. Lin, An electrochemical strategy of doping Fe^{3+} into TiO$_2$ nanotube array films for enhancement in photocatalytic activity. Sol. Energy Mater. Sol. Cells **93**, 1875–1880 (2009). doi:10.1016/j.solmat.2009.07.001
19. M.S. Nahar, J. Zhang, K. Hasegawa, S. Kagaya, S. Kuroda, Mater. Sci. Semicond. Process. **12**, 168–174 (2009). doi:10.1016/j.mssp.2009.09.011
20. C.-H. Chiou, R.-S. Juang, Photocatalytic degradation of phenol in aqueous solutions by Pr-doped TiO$_2$ nanoparticles. J. Hazard. Mater. **149**, 1–7 (2007). doi:10.1016/j.jhazmat.2007.03.035

21. W. Qiu, Y. Zheng, A comprehensive assessment of supported titania photocatalysts in a fluidized bed photoreactor: photocatalytic activity and adherence stability. Appl. Catal. B **71**, 151–162 (2007). doi:10.1016/j.apcatb.2006.08.021

22. A. Fernández, G. Lassaletta, V.M. Jiménez, A. Justo, A.R. González-Elipe, J.-M. Herrmann, H. Tahiri, Y. Ait-Ichou, Preparation and characterization of TiO_2 photocatalysts supported on various rigid supports (glass, quartz and stainless steel). Comparative studies of photocatalytic activity in water purification. Appl. Catal. B Environ. **7**, 49–63 (1995). doi:10.1016/0926-3373(95)00026-7

23. J.G. McEvoya, W. Cuib, Z. Zhang, Degradative and disinfective properties of carbon-doped anatase–rutile TiO_2 mixtures under visible light irradiation. Catal. Today **207**, 191–199 (2013). doi:10.1016/j.cattod.2012.04.015

24. D.B. Black, E.G. Lovering, Estimation of the degree of crystallinity in digoxin by X-ray and infrared methods. J. Pharm. Pharmacol. **29**, 684–687 (1977). doi:10.1111/j.2042-7158.1977.tb11435.x

25. R.D. Shannon, Revised effective ionic radii and systematic studies of interatomic distances in halides and chalcogenides. Acta Crystallogr. **A32**, 751–767 (1976). doi:10.1107/S0567739476001551

26. G. Leofanti, M. Padovan, G. Tozzola, B. Venturelli, Surface area and pore texture of catalysts. Catal. Today **41**, 207–219 (1998). doi:10.1016/S0920-5861(98)00050-9

27. S. Rahimnejad, S. Rahman Setayesh, M.R. Gholami, A credible role of copper oxide on structure of nanocrystalline mesoporous titanium dioxide. J. Iran. Chem. Soc. **5**(3), 367–374 (2008). doi:10.1007/BF03245990

28. E.M. Kalhori, K. Yetilmezsoy, N. Uygur, M. Zarrabi, R.M.A. Shmeis, Modeling of adsorption of toxic chromium on natural and surface modified lightweight expanded clay aggregate (LECA). Appl. Surf. Sci. **287**, 428–442 (2013). doi:10.1016/j.apsusc.2013.09.175

29. L. Amado, A. Albuquerque, A.E. Santo, Influence of stormwater infiltration on the treatment capacity of a LECA-based horizontal subsurface flow constructed wetland. Ecol. Eng. **39**, 16–23 (2012). doi:10.1016/j.ecoleng.2011.11.009

30. H. Amiri, N. Jaafarzadeh, M. Ahmadi, S.S. Martínez, Application of LECA modified with Fenton in arsenite and arsenate removal as an adsorbent. Desalination **272**, 212–217 (2011). doi:10.1016/j.desal.2011.01.018

31. S.B. Bonabi, J.K. Khabushan, R. Kahani, A.H. Raouf, Fabrication of metallic composite foam using ceramic porous spheres "Light Expanded Clay Aggregate" via casting process. Mater. Des. **64**, 310–315 (2014). doi:10.1016/j.matdes.2014.07.061

32. R.K. Tabase, D. Liu, A. Feilberg, Chemisorption of hydrogen sulphide and methanethiol by light expanded clay aggregates (Leca). Chemosphere **93**, 1345–1351 (2013). doi:10.1016/j.chemosphere.2013.07.068

33. M.A. Nkansah, A.A. Christy, T. Barth, G.W. Francis, The use of lightweight expanded clay aggregate (LECA) as sorbent for PAHs removal from water. J. Hazard. Mater. **217–218**, 360–365 (2012). doi:10.1016/j.jhazmat.2012.03.038

34. M. Malakootian, J. Nouri, H. Hossaini, Removal of heavy metals from paint industry's wastewater using Leca as an available adsorbent. Int. J. Environ. Sci. Technol. **6**, 183–190 (2009). doi:10.1007/BF03327620

35. S.-Y. Lee, S.-J. Park, TiO_2 photocatalyst for water treatment applications. J. Ind. Eng. Chem. **19**, 1761–1769 (2013). doi:10.1016/j.jiec.2013.07.012

36. H.J. Choi, M. Kang, Hydrogen production from methanol/water decomposition in a liquid photosystem using the anatase structure of Cu loaded TiO_2. Int. J. Hydrog. Energy **32**, 3841–3848 (2007). doi:10.1016/j.ijhydene.2007.05.011

37. T. Sato, M. Taya, Copper-aided photo-sterilization of microbial cells on TiO_2 film under irradiation from a white light fluorescent lamp. Biochem. Eng. J. **30**, 199–204 (2006). doi:10.1016/j.jeurceramsoc.2009.04.016

38. H.W.P. Carvalhoa, A.P.L. Batistab, P. Hammer, T.C. Ramalho, Photocatalytic degradation of methylene blue by TiO_2–Cu thin films: theoretical and experimental study. J. Hazard. Mater. **184**, 273–280 (2010). doi:10.1016/j.jhazmat.2010.08.033

39. T. Sreethawong, S. Yoshikawa, Immobilization of TiO_2 and Fe–C–TiO_2 photocatalysts on the cotton material for application in a flow photocatalytic reactor for decomposition of phenol in water. Catal. Commun. **6**, 661–668 (2005). doi:10.1016/j.catcom.2005.06.004

40. B. Tryba, Immobilization of TiO_2 and Fe–C–TiO_2 photocatalysts on the cotton material for application in a flow photocatalytic reactor for decomposition of phenol in water. J. Hazard. Mater. **151**, 623–627 (2008). doi:10.1016/j.jhazmat.2007.06.034

41. C.L. Suen, A. Adesina, Aqueous phase oxidative degradation of 4-hydroxy nitrobenzene over a CuO–TiO_2 Catalyst. Asia Pac. J. Chem. Eng. **6**, 85–100 (1998). doi:10.1002/apj.5500060106

42. A.Y. Shan, T.I.M. Ghazi, S.A. Rashid, Immobilisation of titanium dioxide onto supporting materials in heterogeneous photocatalysis: a review. Appl. Catal. A Gen. **389**, 1–8 (2010). doi:10.1016/j.apcata.2010.08.053

43. S. Singh, H. Mahalingam, P.K. Singh, Polymer-supported titanium dioxide photocatalysts for environmental remediation: a review. Appl. Catal. A Gen. **462–463**, 178–195 (2013). doi:10.1016/j.apcata.2013.04.039

44. A. Nezamzadeh-Ejhieh, Z. Salimi, Heterogeneous photodegradation catalysis of o-phenylenediamine using CuO/X zeolite. Appl. Catal. A **390**, 110–118 (2010). doi:10.1016/j.apcata.2010.09.038

45. Z. Sun, Y. Yan, G. Zhang, W. Zhaoyang, S. Zheng, The influence of carriers on the structure and photocatalytic activity of TiO_2/diatomite composite photocatalysts. Adv. Powder Technol. **26**, 595–601 (2015). doi:10.1016/j.apt.2015.01.007